Valence Bond Concepts Applied to the Molecular Mechanics Description of Molecular Shapes. 4. Transition Metals with π-Bonds

Timothy K. Firman and Clark R. Landis*

Contribution from the Department of Chemistry, University of Wisconsin-Madison, 1101 University Avenue, Madison, Wisconsin 53706

Received July 14, 2000

Abstract: We have developed a model for understanding the shapes of transition metal complexes containing multiple bonds. This model, which focuses on Lewis-like structures and the balance of forces arising from σ- and π-bond frameworks, provides a simple method for predicting the structures of transition metal complexes with π-bonds. Potential energy expressions suitable for implementation in molecular mechanics computations have been derived from consideration of orbital hybridizations and coded into our UFF2-based molecular mechanics program, VALBOND. The VALBOND method correctly predicts the structures for a wide variety of experimentally and computationally characterized compounds containing metal–ligand multiple bonds.

Introduction

For the last 70 years, understanding the shapes of molecules has played an important role in the development and assessment of simple bonding models.[1–4] In the past four decades, molecular orbital (MO) theory[4–6] and valence shell electron pair repulsion (VSEPR) theory[7–12] have provided the most potent models for understanding molecular shapes. A useful review of methods for rationalizing molecular shapes is provided by Burdett's pink book.[4] Recently, we have shown that a simple valence bond (VB)-influenced model successfully describes the geometries of main group molecules[13,14] and a variety of transition metal hydrides and alkyls.[15–19] For transition metal complexes with predominately covalent bonding, this model applies common concepts, such as hybridization and resonance, to rationalize molecular shapes. We have shown that these concepts are

consistent with electron density distributions obtained from high-level ab initio computations and form the basis of novel, useful molecular mechanics algorithms. In this paper we demonstrate the extension of this simple bonding model and its molecular mechanics formulation to transition metal complexes containing metal–ligand and metal–metal multiple bonds.

Complexes with multiple bonds between transition metals and carbon, nitrogen, and oxygen are ubiquitous and play important roles in many reactions of significant importance to industrial processes and living organisms. Not surprisingly, a vast literature chronicles computational and empirical investigations of metal–ligand multiple bonds.[20] Seminal descriptions of the electron structure of complexes with metal–carbon multiple bonds come from the work of Taylor and Hall,[21] Cundari and Gordon,[22–26] Hoffmann,[27] and Rappé, Goddard, and Carter[28–33] and have been expanded upon by others.[34–38] Oxo, imido, and nitrido com-

(1) Pauling, L. *J. Am. Chem. Soc.* **1931**, *53*, 1367–1400.
(2) Pauling, L. *The Nature of the Chemical Bond*; Cornell University: Ithaca, 1960.
(3) Slater, J. C. *Phys. Rev.* **1931**, *37*, 481–494.
(4) Burdett, J. K. *Molecular Shapes*; John Wiley and Sons: New York, 1980.
(5) Albright, T. A.; Burdett, J. K.; Whangbo, M. H. *Orbital Interactions in Chemistry*; John Wiley and Sons: New York, 1985.
(6) Bartell, L. S.; Plato, V. *J. Am. Chem. Soc.* **1973**, *95*, 3097–3104.
(7) Gillespie, R. J. *Molecular Geometry*; Van Nostrand Reinhold: London, 1972.
(8) Gillespie, R. J.; Hargittai, I. *The VSEPR Model of Molecular Geometry*; Allyn and Bacon: Boston, 1991.
(9) Gillespie, R. J. *Chem. Soc. Rev.* **1992**, 59.
(10) Gillespie, R. J. *J. Chem. Educ.* **1992**, *69*, 116.
(11) Gillespie, R. J.; Robinson, E. A. *Inorg. Chem.* **1995**, *34*, 978.
(12) Kepert, D. L. *Inorganic Stereochemistry*; Springer-Verlag: Berlin, 1982.
(13) Cleveland, T.; Landis, C. R. *J. Am. Chem. Soc.* **1996**, *118*, 6020–6030.
(14) Root, D. M.; Landis, C. R.; Cleveland, T. *J. Am. Chem. Soc.* **1993**, *115*, 4201–4209.
(15) Firman, T. K.; Landis, C. R. *J. Am. Chem. Soc.* **1998**, *120*, 12650–12656.
(16) Landis, C. R.; Cleveland, T.; Firman, T. K. *J. Am. Chem. Soc.* **1995**, *117*, 1859–1860.
(17) Landis, C. R.; Cleveland, T.; Firman, T. K. *Science* **1996**, *272*, 179.
(18) Landis, C. R.; Cleveland, T.; Firman, T. K. *J. Am. Chem. Soc.* **1998**, *120*, 2641–2649.
(19) Landis, C. R.; Firman, T. K.; Root, D. M.; Cleveland, T. *J. Am. Chem. Soc.* **1998**, *120*, 1842–1854.

(20) Nugent, W. A.; Mayer, J. M. *Metal-Ligand Multiple Bonds*; John Wiley and Sons: New York, 1988.
(21) Taylor, T. E.; Hall, M. B. *J. Am. Chem. Soc.* **1984**, *106*, 1576–1584.
(22) Cundari, T. R.; Gordon, M. S. *J. Am. Chem. Soc.* **1991**, *113*, 5231–5243.
(23) Cundari, T. R.; Gordon, M. S. *J. Am. Chem. Soc.* **1992**, *114*, 539–548.
(24) Cundari, T. R.; Gordon, M. S. *Organometallics* **1992**, *11*, 55–63.
(25) Gordon, M. S.; Cundari, T. R. *Coord. Chem. Rev.* **1996**, *147*, 87–115.
(26) Musaev, D. G.; Morokuma, K.; Koga, N.; Nguyen, K. A.; Gordon, M. S.; Cundari, T. R. *J. Phys. Chem.* **1993**, *97*, 11435–11444.
(27) Goddard, R. J.; Hoffmann, R.; Jemmis, E. D. *J. Am. Chem. Soc.* **1980**, *102*, 7667–7676.
(28) Carter, E. A.; Goddard, W. A. *J. Am. Chem. Soc.* **1986**, *108*, 4746–4754.
(29) Carter, E. A.; Goddard, W. A. *J. Am. Chem. Soc.* **1987**, *109*, 579–580.
(30) Carter, E. A.; Goddard, W. A. *Organometallics* **1988**, *7*, 675–686.
(31) Carter, E. A.; Goddard, W. A. *J. Phys. Chem.* **1988**, *92*, 5679–5683.
(32) Irikura, K. K.; Goddard, W. A. *J. Am. Chem. Soc.* **1994**, *116*, 8733–8740.
(33) Rappé, A. K.; Goddard, W. A. *J. Am. Chem. Soc.* **1982**, *104*, 448–456.
(34) Cauchy, D.; Volatron, F.; Jean, Y. *New J. Chem.* **1994**, *18*, 191–196.
(35) Heinemann, C.; Schwarz, H.; Koch, W.; Dyall, K. G. *J. Chem. Phys.* **1996**, *104*, 4642–4651.

Scheme 1
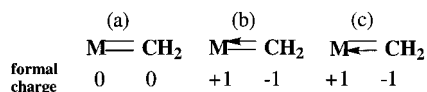
Scheme 2
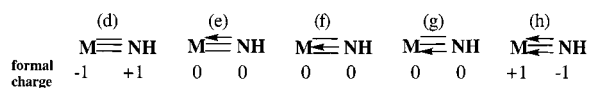
plexes commonly are thought to exhibit similar bonding patterns as shown in theoretical investigations by Goddard and Rappé,[27-32,39] Hall and Lin,[40] Cundari et al.,[25,41-44] and others.[45-47] Recently, Kaupp[48] has provided insight into the electronic structure underlying the peculiar geometries of some tetraalkyl oxo complexes and has explored the influence of π-bonding on the structures of d^0 metal complexes.

Analyses of metal−ligand multiple bonds in terms of localized bonding models are relatively recent. Goddard and co-workers[28-30,32,33,39,49] emphasized simple electron-pair coupling in the formation of metal−ligand π-bonds based on the results of GVB-PP computations. Cundari and Gordon[25] have applied MCSCF/LMO/CI computations to assess the contributions of multiple resonance structures to metal−ligand multiple bonds. They found that metal alkylidene and metal silylidene double bonds to early transition metal complexes are dominated by the three resonance structures shown in Scheme 1. In contrast, early transition metal imido complexes are dominated by the "triple bond" structures shown in Scheme 2. Formally, configurations b and c are "ionic" resonance structures in the sense that covalent bonds in configuration a have been polarized. The bottom-most position of the bond diagram represents the σ-bond, whereas the upper position(s) represent π-bond(s).

Cundari and Gordon conclude that metal−alkylidene bonds of early transition are slightly polarized toward C, with more polarization of the σ-bond than the π-bond. Metal−imido bonds are more strongly polarized, as expected from electronegativity trends. Significantly, Cundari and Gordon conclude that a single configuration does not describe the electronic structure of early transition metal−ligand multiple bonds. More recently, Frenking[50,51] and Kaupp[52-54] have contributed natural bond order

and natural localized molecular orbital analyses of electron density distributions computed for some metal carbene and carbyne complexes. With the exception of recent work by Kaupp, the influence of π-bonding on the shapes of transition metal complexes is not well explored, and a successful localized bonding model has not yet emerged.

Our goal is to develop simple bonding models that account for as much of the electronic structure as possible and that lend themselves to rigorous testing in the form of molecular mechanics implementations. This contribution primarily concerns complexes containing one metal−ligand or metal−metal multiple bond with the remaining metal valency filled by covalent bonds to hydrides and alkyls. Our approach is to extend the VB-like model that has been so successful for describing transition metals containing covalent, single bonds to complexes containing one or two multiple bonds.[15-19,55] We refer to this model as VB-like because it focuses on the application of hybrid orbital directionality and resonance interactions to rationalize molecular structures and because the hybrid orbital descriptors are quite similar to those found in perfect-pairing VB computations. As such, the model is limited to bonding that is predominately covalent. Within that limitation, the model is surprisingly robust and leads to good descriptions of metal complex geometries for difficult cases, such as open shell compounds. We begin by presenting a simple model for estimating a single, dominant resonance configuration for simple complexes containing one or two metal−ligand multiple bonds with a supporting set of alkyl or hydride ligands. We then provide a qualitative model for understanding molecular geometries by considering the balance of forces arising from the σ- and π-bonding frameworks. Approximately 50 structures involving metal−ligand multiple bonds are analyzed in detail. The primary analysis tools are DFT(B3LYP) electronic structure calculations with natural bond orbital[56-60] analysis of the electron density distribution and the VALBOND force field, which is a molecular mechanics program whose algorithms are based on VB concepts.[13,14,16-19,61-63] A large body[16,19,52,61-63] of work convincingly demonstrates that the B3LYP method gives similar geometries to other high level ab initio techniques and accurately reproduces experimental geometries of transition metal hydrides and alkyls. A final note concerns multiple local minima that occur frequently in simple metal alkyl and hydride complexes. Using either VALBOND or DFT(B3LYP) computations multiple minima have been found for many of the complexes shown herein. In the interest of brevity, in this contribution we present only the lowest energy structures.

Lewis Structures and Hybridization for Complexes with Metal−Ligand Multiple Bonds. The electronic structures of metal−ligand multiple bonds for naked metal diatomics have

(36) Fox, H. H.; Schofield, M. H.; Schrock, R. R. *Organometallics* **1994**, *13*, 2804−2815.

(37) Marquez, A.; Sanz, J. F. *J. Am. Chem. Soc.* **1992**, *114*, 10019−10024.

(38) Schrock, R. R.; Crowe, W. E.; Bazan, G. C.; Dimare, M.; Oregan, M. B.; Schofield, M. H. *Organometallics* **1991**, *10*, 1832−1843.

(39) Rappé, A. K.; Goddard, W. A. *J. Am. Chem. Soc.* **1982**, *104*, 3287−3294.

(40) Lin, Z. Y.; Hall, M. B. *Coord. Chem. Rev.* **1993**, *123*, 149−167.

(41) Benson, M. T.; Cundari, T. R.; Moody, E. W. *J. Organomet. Chem.* **1995**, *504*, 1−13.

(42) Benson, M. T.; Bryan, J. C.; Burrell, A. K.; Cundari, T. R. *Inorg. Chem.* **1995**, *34*, 2348−2355.

(43) Benson, M. T.; Cundari, T. R.; Lim, S. J.; Nguyen, H. D.; Piercebeaver, K. *J. Am. Chem. Soc.* **1994**, *116*, 3955−3966.

(44) Cundari, T. R. *J. Am. Chem. Soc.* **1992**, *114*, 7879−7888.

(45) Cayton, R. H.; Chisholm, M. H.; Davidson, E. R.; Distasi, V. F.; Du, P.; Huffman, J. C. *Inorg. Chem.* **1991**, *30*, 1020−1024.

(46) Pyykkö, P.; Tamm, T. *J. Phys. Chem. A* **1997**, *101*, 8107−8114.

(47) Brower, D. C.; Templeton, J. L.; Mingos, D. M. P. *J. Am. Chem. Soc.* **1987**, *109*, 5203−5208.

(48) Kaupp, M. *Eur. J. Chem.* **1998**, *4*, 2059−2071.

(49) Carter, E. A.; Goddard, W. A. *J. Phys. Chem.* **1988**, *92*, 2109−2115.

(50) Frenking, G.; Vyboishchikov, S. F. *Eur. J. Chem.* **1998**, *4*, 1428−1438.

(51) Frenking, G.; Vyboishchikov, S. F. *Eur. J. Chem.* **1998**, *4*, 1439−1448.

(52) Kaupp, M. *Eur. J. Chem.* **1998**, *4*, 2059−2071.

(53) Kaupp, M. *Eur. J. Chem.* **1999**, *5*, 3631−3643.

(54) Kaupp, M. *Angew. Chem., Int. Ed.* **1999**, *38*, 3035−3036.

(55) Landis, C. R.; Firman, T. K.; Cleveland, T.; Root, D. M. *NATO Adv. Study Inst. Ser., Ser. 3* **1997**, *41*, 49−75.

(56) Foster, J. P.; Weinhold, F. *J. Am. Chem. Soc.* **1980**, *102*, 7211−7218.

(57) Carpenter, J. E.; Weinhold, F. *J. Am. Chem. Soc.* **1988**, *110*, 368−372.

(58) Reed, A. E.; Weinstock, R. B.; Weinhold, F. *J. Chem. Phys.* **1985**, *83*, 735−746.

(59) Glendening, E. D.; Badenhoop, J. K.; Reed, A. E.; Carpenter, J. E.; Weinhold, F. *NBO 4.0*; University of Wisconsin: Madison, WI, 1994.

(60) Suidan, L.; Badenhoop, J. K.; Glendening, E. D.; Weinhold, F. *J. Chem. Educ.* **1995**, *72*, 583−586.

(61) Kaupp, M. *J. Am. Chem. Soc.* **1996**, *118*, 3018−3024.

(62) Siegbahn, P. E. M.; Blomberg, M. R. A.; Svensson, M. *J. Am. Chem. Soc.* **1993**, *115*, 4191−4200.

(63) Ogliaro, F.; Loades, S. D.; Cooper, D. L.; Karadakov, P. B. *J. Phys. Chem. A* **2000**, *104*, 7091−7098.

been investigated in great detail. Goddard and co-workers provide the seminal descriptions of metal−ligand multiple bonds from a VB perspective. Rappè and Goddard[33,39] described Cl4-CrO as four polar electron pair bonds between Cr and Cl with the remaining two Cr electrons couple with four electrons on O to make two covalent Cr−O π-bonds and a donor acceptor σ-bond, similar to CO. In Cl_2CrO_2, two of the six Cr electrons make polar electron pair bonds to Cl, and the remaining electrons spin pair to make Cr=O double bonds. Carter and Goddard[49] considered the nature of early and late transition metal−oxo bonds in the naked diatomics VO^+ and RuO^+. The ground triplet state of VO^+ is described as triple bond, similar to that of Cl_4CrO, whereas the ground quartet state of RuO^+ involves a covalent σ-bond and two three-electron π-bonds, similar to the bonding in O_2. With respect to M=CH_2 bonding numerous descriptions of "naked" complexes have been provided.[32,63] Metal complexes with saturated valences and M=C bonds are our primary concern. Goddard and Carter[30] described a VB analysis of $ClRu(CH_2)H$ with an emphasis on two conformers: one with the C−Ru−H plane orthogonal to the H−C−H plane and one with the two planes parallel. The former structure, which is lower in energy, is a 12-electron complex with two Ru lone pairs, three Ru σ-bonds (to Cl, H, and C), and one Ru−C π-bond. Most relevant to the subject of this contribution, Goddard and Carter identified the C−Ru−H bond angle of 90° to be a requirement of maintaining orthogonality among the Ru−C and Ru−H σ-bonds and the Ru−C π-bond.

We have shown that simple rules may be used to establish Lewis-like structures and hybridizations for both main group and transition metal compounds.[19] Focusing on transition metal complexes, the rules may be summarized as:

1. The d-block elements form sd^{n-1} hybrids, where n is the number of electron pairs (or for open shells, the number of electron pairs plus the number of unpaired electrons) at the metal center.

2. The hybridization of metal-centered lone pairs, radicals, and π-bonds is essentially pure d.

3. Complexes with electron counts greater than 12 are hypervalent. Hypervalent complexes are dominated by three center-four electron bonding which maximizes at linear arrangements of the terminal centers.

For complexes dominated by *covalent* metal−ligand bonding, the rules listed above provide a robust "zeroth-order" description of the electron density distribution of the molecule and a solid basis for predicting the molecular shapes. Our previous work has shown that, for a wide variety of transition metals and hydrides, these rules (1) allow one to rationalize the unusual coordination geometries, often involving several local minima, of transition metal hydrides and alkyls which can include open as well as closed shell, (2) are consistent with geometries and electron density distributions computed at HF, MP2, GVB, and DFT(B3LYP) levels, (3) effectively make use of the idea of hypervalency and three-center−four-electron bonding interactions to rationalize geometries and make a strong connection with geometries and electronic structures of hypervalent main group compounds. For >12 electron counts at the metal, we de-emphasize the role of metal valence p orbitals in favor of three-center−four-electron interactions.

A useful, general procedure for obtaining the Lewis-like structure when metal−ligand multiple bonds are present is the following:

(A) Initially draw a structure with metal−ligand single bonds and a full octet for all ligands. Some examples are shown below:


	(CH2)ReH3	(CH)WH3	(N)OsH3	(O)IrH3	(CH2)2WH2
Formal Charge on π-bound L	-1	-2	-2	-1	-1
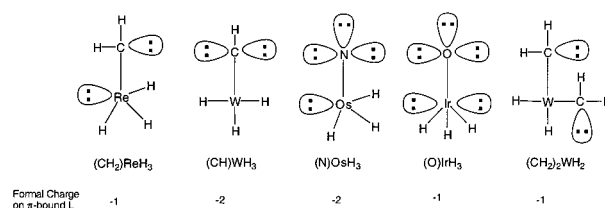
(B) If the metal uses fewer than six orbitals and the ligand-(s) have suitable lone pairs, remove a ligand lone pair and draw an additional metal−ligand bond. This leads to the following Lewis-like structures, each with sd^3 hybridization in the σ-bonding framework:

	(CH2)ReH3	(CH)WH3	(N)OsH3	(O)IrH3	(CH2)2WH2
Formal charge of π-bound L	0	0	-1	-1	0
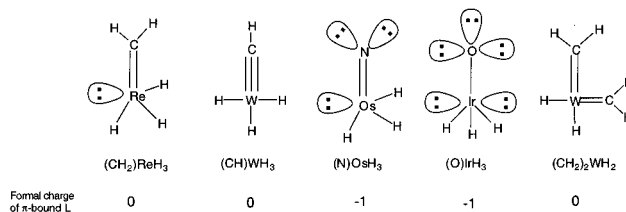
(C) Formal charges, which have *no* physical meaning and are *not* equivalent atomic partial charges, are useful for choosing among alternative resonance configurations. As a general guide, the formal charges of ligands making covalent π-bonds at a metal will be either 0 or −1. Because oxygen is much more electronegative than transition metals, a formal charge of +1 at O is unlikely. In consequence, *purely covalent* M≡O triple bonds are unlikely (see **A** below). At the other extreme, N and C lack the electronegativity to support −2 and −1 formal charges, respectively. In consequence, singly bonded metal nitrides (such as **B**) and singly bonded metal−alkylidenes (such as **C**) are not expected.
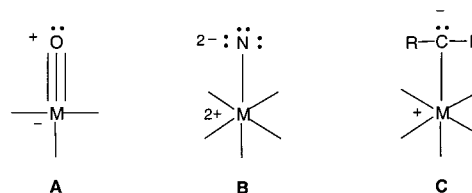
The shapes of optimal σ-bonding and π-bonding metal orbitals are different. The sd^n hybrids which make optimal σ-bonds are both cylindrically- and centro-symmetric. In contrast, optimal π-bonding metal orbitals are pure d and have a "cloverleaf" shape.

sd¹ hybrid   sd³ hybrid   sd∞ (pure d)
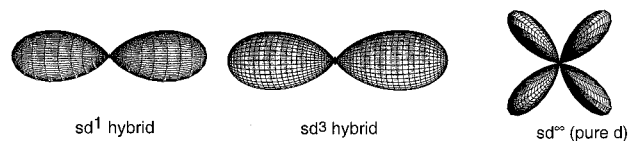
In discussing hybridization it is useful to recall that the symbols sd^1 and sd^3 indicate orbitals that have 50 and 75% d-character, respectively. In the next section, we examine the impact of these orbital shapes on the geometries of three simple transition metal complexes.

Metal−Ligand σ- and π-Bonding: Balance of Forces in XMH$_3$ Complexes. As a simple teaching set, consider the oxo complex, $OIrH_3$, and the two nitride complexes, NWH_3 and $NOsH_3$. According to our prescriptions, all of these complexes will utilize sd^3 hybridization in the σ-bonding framework. The Lewis-like structures of $OIrH_3$, $NOsH_3$, and NWH_3 differ in
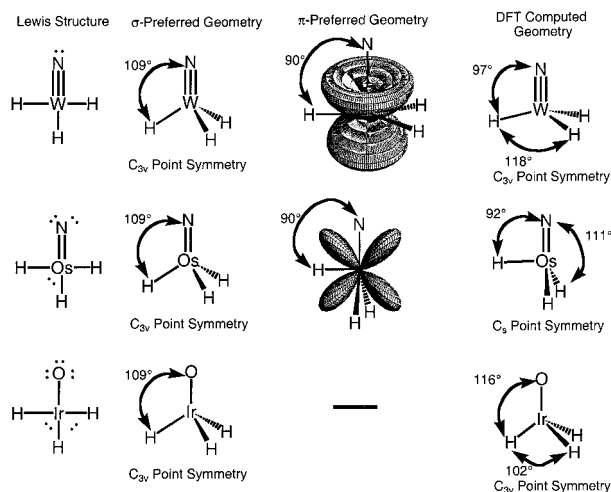
Figure 1. Illustration of the balance between optimization of σ- and π-bonding the complexes OIrH₃, NWH₃, and NOsH₃.
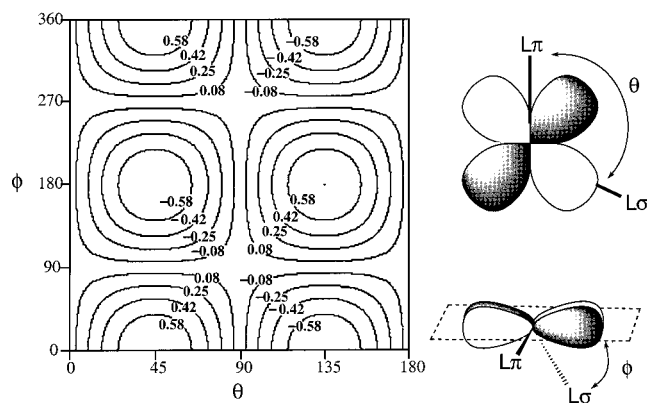

Figure 2. Contour plot of overlap between a metal-centered sd^n-hybridized σ-bond hybrid that connects the metal and L$_\sigma$ (this centrosymmetric orbital has its axis located on the M–L$_\sigma$ vector and is not shown explicitly) and a dπ orbital (shown explicitly as L$_\sigma$ is moved along the spherical angles θ and φ.

the number of π-bonds: the O–Ir linkage bond has only a σ-bond, the N=Os linkage has one π-bond, and N≡W comprises two π-bonds. We consider the molecular shape to be that which minimizes the overlaps (or nonorthogonalities in Pauling's terminology[64]) of the bond-forming orbitals; the observed molecular geometries are those which best balance all forces arising from the metal-centered sd³ σ-bond hybrids and the pure d π-bond orbitals. As illustrated in Figure 1, consideration of the sd³-hybridized σ-bonding framework, only, leads to an idealized structure of a tetrahedron (the ground-state geometry of sd³-hybridized metal hydrides such as triplet WH₄ and singlet OsH₄). The tetrahedral geometry minimizes overlap among the sd³ hybrids, which have nodal cone angles of 71° and 109° with respect to the orbital axis. The geometry of OIrH₃, which is σ-bonding only by our simple rules, should have bond angles close to 109°, with some modification due to the different electronegativities of O and H. As shown in Figure 1, such a geometry is found by DFT(B3LYP) computation.

For NOsH₃ our rules yield an Os center with four σ-bonds (sd³ hybridization), one lone pair (pure d), and one π-bond (pure d). A plot of the overlap of the metal-centered part of a M–L$_\sigma$ bond and a M–L$_\pi$ orbital as a function of polar angles is given in Figure 2. As a result of sd³ hybridization the σ-preferred geometry of NOsH₃ is tetrahedral. However, the π-preferred geometry is one that places the M–H bonds in the nodes of the dπ orbital; consequently the hydrogen that lies in the plane

Table 1. DFT(B3LYP) and VALBOND Optimized Geometries for XMH₃ Complexes with an M≡X Triple Bond (X = HC-, HN-, N-, O-)

[(NH)WH₃]⁺	DFT	VALBOND[a]	[OWH₃]⁺	DFT	VALBOND[a]
W-N	1.68 Å	1.53 Å	W-O	1.65 Å	1.43 Å
W-H	1.69 Å	1.72(1) Å	W-H	1.69 Å	1.73(1)Å
N-W-H	96°	94 (1)°	O-W-H	98°	94(1)°
H-W-H	118°	120°	H-W-H	118°	120°
W-N-H	180°	180°			

(CH)WH₃	DFT	VALBOND[a]	NMoH₃	DFT	VALBOND[a]
W-C	1.74 Å	1.56 Å	Mo-N	1.64 Å	1.48 Å
W-H	1.72 Å	1.73 Å	Mo-H	1.71 Å	1.68 Å
C-W-H	97°	94(1)°	N-Mo-H	97°	92(1)°
H-W-H	118°	120°	H-Mo-H	118°	120°
H-C-W	180°	180°			

[a] The numbers in parentheses represent average deviations for the given internal coordinate.

of the dπ orbital will be forced to near 90° N–Os–H bond angle(s). Illustration of a structure that is consistent with both σ- and π-bond preferences is provided in Figure 1. The DFT-(B3LYP)-computed structure of NOsH₃ clearly demonstrates that *the presence of a single, localized π-bond correlates with a low-symmetry structure despite the lack of any other symmetry-lowering attachments to the N!* The DFT(B3LYP)-computed structure of NOsH₃ can be viewed as a compromise between forces arising from overlaps within the σ- and π-bond frameworks.

As shown in Figure 1, the two π-bonds of NWH₃ form a cylinder of electron density about the W–N axis. Maximization of π-bonding places the W–H bonds in the plane that is perpendicular to the W–N axis (an alternative location would be opposite the W–N bond; however, this arrangement would create extensive overlap with the W–N σ-bond). The DFT-(B3LYP) structure, which exhibits N–W–H bond angles of 97° and H–W–H bond angles of 118°, consistent with a structure that lies between the σ-preferred and π-preferred geometries of Figure 1.

In addition to the main group ligands described above, this localized bonding model also applies to transition metal–transition metal bonds. Lewis structures for three metal–metal bonded dimers (H₃Os–OsH₃, H₃Re=ReH₃, and H₃W≡WH₃) are shown below. As a consequence, we expect the coordination geometries about the metal centers of H₃Os–OsH₃, H₃Re=ReH₃, and H₃W≡WH₃ to parallel those of O–IrH₃, N=OsH₃, and HC≡WH₃. As we will show, this expectation is realized with surprising fidelity.

In the following sections we analyze the details of the electronic and geometric structures of complexes using NBO analysis (to examine electron density distributions) and VALBOND molecular mechanics (to examine force balance between simple models of σ- and π-bonding). We examine (1) XML₃

(64) Pauling, L. *Proc. Natl. Acad. Sci. U.S.A.* **1976**, *73*, 274–275.
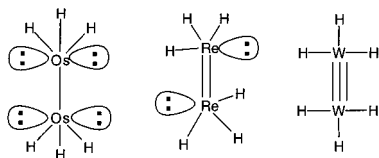
complexes in the order of XM triple bonds, double bonds, and then single bonds, (2) metal−metal bonded dimers of the formula M_2H_6 (3) XML_4 complexes, starting with XM double bonds, and (4) X_2ML_2 complexes with the goal of exploring the impact of π-bonds to two different ligands.

XML_3 Complexes: Computed and Experimental Structures. Triple-Bonded $X{\equiv}MH_3$. We have examined a series of compounds: $(HN)WH_3^+$, OWH_3^+, $HCWH_3$, $NMoH_3$, NWH_3, $(HC)WH_3$, and $OVMe_3$. Each of these compounds can be described as having a $X{\equiv}M$ triple bond according to our Lewis-like model. The DFT(B3LYP) and VALBOND-optimized geometries are presented in Table 1, and the NBO analyses of DFT(B3LYP) density matrixes are summarized in Table 2.

The DFT(B3LYP)-computed geometries of the $X{\equiv}MH_3$ complexes all exhibit C_{3v} point group symmetries and X−M−H bond angles of about 98°. As shown by the data in Table 1, the VALBOND computations, which have no specific parametrization for the compounds examined here and use a default equal-weighting of forces arising from nonorthogonalities in the idealized σ-bond and π-bonds, yield structures that are quite similar to the DFT(B3LYP) structures. The differences are (1) a weak symmetry-breaking in the VALBOND computations that yields X−M−H angles that differ by ca. 2° from axial symmetry (2) X−M−H angles that are ca. 4° smaller than the DFT-(B3LYP) values, and (3) significantly shorter $X{\equiv}M$ bonds than found by DFT(B3LYP). The shortened $X{\equiv}M$ bonds and the systematically small X−M−H angles are due to the use of

default parameters in the VALBOND/UFF program as described in the Computational Details section. Because our goal is to test bonding ideas rather than to optimize force field behavior, we accept these differences and resist further parameter optimization.

For each triple-bonded complex, the best single NBO[56−58] configuration corresponds to that predicted by our Lewis-like model. A single NBO configuration describes these electron densities well, accounting for >99.7% of the total electron density with high occupancies (1.9−2.0 electrons) of all localized orbitals. The NBO bond orbitals for M−X bonds are substantially polar. Hence, the fact that a single NBO configuration describes most of the electron density does not imply that the bonds are purely covalent and is not in conflict with the multiple configuration descriptions of Cundari and Gordon.[25] In each case the natural charge[58] on the transition metal was close to +1, and the triple bonded atom (X) had a partial negative charge (ranging from −0.31 to −0.51). In keeping with the expected sd^3 metal atom hybridization in the σ-bonding framework, the average hybridization of the metal atoms is $sd^{2.9}$. The metal atom allocates more d character to the M−X bond than it does to each of the M−H bonds. As we have shown previously,[19] as the polarity of the M−X σ-bonds increases, the d character of the M−H bonds decreases and that of the M−X bond increases. We have attributed this trend to the increasing participation of MH_x^{y+} X^- resonance configurations as the electronegativity of X increases.
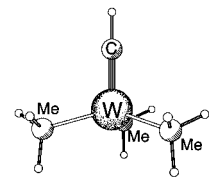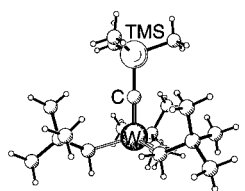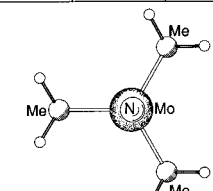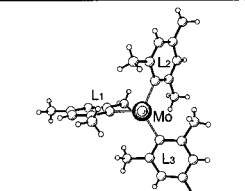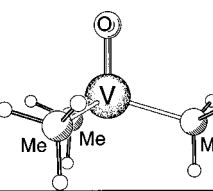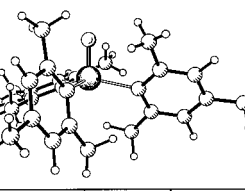
Highly polar X−M bonds can lead to apparently high formal charges. For example, the complexes $O{\equiv}VMe_3$ and $O{\equiv}WH_3^+$ have oxygen formal charges of +1 when the Lewis structures are formulated with purely covalent $O{\equiv}M$ triple bonds. Of course, the bonds are highly polar, and the formal charge bears no semblance to the charge distributions. These examples serve

Table 2. NBO Analyses of $X{=}MH_3$ Complexes

Compound	NPA Charges			M σ-Bond NBO's		M-X π NBO	X-H/LP NBO	%Lewis Density
	M	X	L(x3)	M-X	M-L			
$HN{\equiv}WH_3^+$	+1.27	-0.06	-0.07	28%W;sd$^{3.3}$ 72%N;sp$^{0.8}$	47%W;sd$^{2.9}$ 53% H; s	35%W 65%N	72%N;sp$^{1.2}$ 28% H; s	99.8%
$O{\equiv}WH_3^+$	+1.51	-0.34	-0.06	29%W;sd$^{3.3}$ 71%N;sp$^{4.8}$	47%W;sd$^{2.6}$ 53% H; s	27%W 73%O	100%O;sp$^{0.2}$	99.8%
$HC{\equiv}WH_3$	+0.76	-0.16	-0.20	37%W;sd$^{2.98}$ 63%C;sp$^{0.8}$	40%W;sd$^{3.0}$ 60% H; s	52%W 48%C	59%C;sp$^{1.2}$ 41% H; s	99.8%
$N{\equiv}MoH_3$	+0.72	-0.31	-0.14	42%Mo;sd$^{5.0}$ 58%N;sp$^{4.7}$	43%Mo;sd$^{2.6}$ 57% H; s	46%Mo 54%N	100%N;sp$^{0.2}$	99.5%
$N{\equiv}WH_3$	+1.0	-0.44	-0.19	41%W;sd$^{4.4}$ 59%N;sp$^{4.5}$	40%W;sd$^{2.7}$ 60% H; s	43%W 57%N	100%N;sp$^{0.2}$	99.9%
$HC{\equiv}WMe_3$	+1.12	-0.13	-0.33	36%W;sd$^{2.7}$ 64%C;sp$^{0.8}$	32%W;sd$^{3.0}$ 64% C; sp$^{3.1}$	53%W 47%C	59%C;sp$^{1.2}$ 41% H; s	99.5%
$O{\equiv}VMe_3$	+1.02	-0.41	-0.22	27%V;sd$^{5.6}$ 73%O;sp$^{4.5}$	35%V;sd$^{2.5}$ 65%C;sp$^{4.1}$	25%V 75%O	O; sp$^{0.2}$	99.8%

^{a} Atom-centered charges based on natural population analysis (see ref 58). ^{b} The percent contribution of each atom-centered hybrid to the σ natural bond and the hybrid orbital compositions are given (see ref 58). ^{c} The percent contribution of the metal-centered d orbital and the ligand-centered p-orbital to the π natural bond is given. ^{d} The composition and hybridization of L−H σ-bond and a ligand-centered lone pair. ^{e} The percent of the total electron density that is described by a Lewis structure consisting of orbitals, bonds, and lone pairs.

Table 3. Computed (by DFT(B3LYP) and VALBOND) and Experimental Structures for X≡ML₃ Complexes

HC≡WMe₃	DFT	VALBOND	TMSC≡WNp₃	TALTOP[a]	VALBOND
W-CH	1.76 Å	1.73 Å	W-C	1.74 Å	1.74 Å
W-Me	2.11 Å	2.10 Å	W-R	2.10 Å	2.11 Å
C-W-Me	104°	95(1)°	C-W-R	107°	105(1)°
Me-W-Me	115°	119(1)°	R-W-R	112°	114(1)°
H-C-W	180°	180°	W-C-Si	180°	179°

N≡MoMe₃	DFT	VALBOND	N≡Mo(Mesityl)₃	ZAFVIL[a]	VALBOND
Mo-N	1.68 Å	1.48 Å	Mo-N	1.65 Å	1.48 Å
Mo-Me	2.12 Å	2.05 Å	Mo-L₁	2.12(2) Å	2.05 Å
N-Mo-Me	102°	95°	N-Mo-L₁	100(2)°	95(1)°
Me-Mo-Me	116°	120°	L₁-Ir-L₂	118(4)°	119°

O≡VMe₃	DFT	VALBOND	O≡V(Mesityl)₃	SOCLAX[a]	VALBOND
V-O	1.59 Å	1.37 Å	V-O	1.58 Å	1.37 Å
V-Me	2.00 Å	2.10 Å	V-Mes	2.06(3) Å	2.09(1) Å
O-V-Me	112°	95(2)°	O-V-Mes	102(3)°	96(2)°
Me-V-Me	107°	119°	Mes-V-Mes	116(5)°	119°

[a] Six letter Cambridge Structure Database REFCODE citations: TALTOP,[65] ZAFVIL,[66] SOCLAX.[67]

to illustrate that formal charges, per se, are not important or useful when there is a clear choice of the dominant Lewis configuration. Formation of triple bonds transpires to satisfy the valencies of the metal and oxygen.

Empirical structures support the general VALBOND scheme. Although complexes of the type X≡MH₃ have not been characterized experimentally, structures are available for several alkyl derivatives. Structural features obtained from VALBOND computations are compared with experimental[65−67] or DFT-(B3LYP)-computed structures in Table 3; overall the agreement is very good. In these structures we see again that VALBOND computations overemphasize the affect of overlaps between σ- and π-bonds (leading to X−M−R angles that are ca. 7° lower than those observed by experiment) and underestimate X≡M bond lengths because of deficiencies in the default parametrization.

Doubly-Bonded X=ML₃. Unlike HNWH₃⁺, the Lewis-like model of HNReH₃ cannot simultaneously have a HN≡Re triple bond and a normal valent, 12-electron count at the metal. As a result, complexes of the type X=MH₃ exhibit molecular shapes that are strikingly different from those of X≡MH₃ complexes and provide compelling illustrations of the influence of localized

π-bonding on molecular structure. Computational structures and NBO analyses for X=MH₃ complexes are provided in Tables 4 and 5, respectively. These structures fall neatly into two classes: those that are well-described by a single configuration with an X=M double bond (Re alkylidene, imido, and oxo complexes and Ta alkylidenes) and those that require multiple configurations and partial double-bond character (Ir alkylidene, Os alkylidyne, and nitride complexes).

Geometries computed by VALBOND for X=ReH₃ and Ta alkylidene complexes closely match the DFT(B3LYP) results. For the Re complexes, the hydride (H₄) that lies in the plane of the π-bond is positioned near the nodal plane, thus making X−Re−H₄ bond angles near 90°. We note that two of the experimental structures of Ta(neopentylidene)(neopentyl)₂-(trimethylsilyl)[68] and Ta(trimethylsilylmethylidene)(trimethyl-silylmethyl)₂(trimethylsilyl)[69] exhibit C₃ disorder in the crystallographic structures. As a result, the methylidene and methyl groups are not distiguished in the crystallographic structure, and their geometric parameters are averaged. As seen for the X≡MH₃ complexes, the bond-order correction formula underestimates the X=Re lengths, although not so drastically.

The NBO-bonding schemes and the computed structures for all X=ReH₃ complexes closely conform to those prescribed by our VB-like model. Re−H bonds are relatively apolar, but the X−Re bonds have increasing polarity in the expected order: (least polar) H₂C−Re < HN−Re < O−Re (most polar). The average Re−H hybridization ranges from ca. sd²·⁷ for the more covalent alkylidene complex to sd²·⁴ for the oxo complex, in keeping with a greater contribution from ionic resonance structures as the electronegativity of the X group increases (please note that average hybridizations are computed by averaging the %d character of the bonds and then converting that average into sdⁿ hybridizations). The minimized X=ReH₃ complexes exhibit large distortions from axial symmetry with one H (H₄) lying between the lobes of X=Re π-bond and the remaining two H's nearly perpendicular to the plane of the X=Re π-bond. The H−Re−H angles decrease as the polarity of X increases, in keeping with a shift from ca. sd³ hybridization and preferred bond angles of 109° toward sd² hybridization and preferred bond angles of 90°.

The NBO results for H₂C=TaH₃ describe significant polarity in the Ta−H bonds (65% H, 35% Ta) and a high charge (+1.4) on the Ta; these charge distributions are similar to those of TaH₅ and TaMe₅ and are consistent with the low electronegativities of early transition metals.

The Ir alkylidene, (H₂C)IrH₃ can be described by two resonance structures: (1) a normal valent (12 electron) Ir with a C−Ir single bond and a lone pair on the methylidene C or (2) a hypervalent (14 electron) complex with a C=Ir double bond and one 3-center−4-electron (3c-4e⁻) H−Ir−H bond. The former resonance structure has sd³ hybridization in the σ-bond framework, no C−Ir π-bond, one lone pair, a −1 formal charge on the C, and a +1 formal charge on the metal. The latter resonance configuration has sd² hybridization in the σ-bond framework, one C−Ir π-bond, formal charges of −0.5 on each of the two hydrides participating in 3c-4e⁻ bonding, and a +1 formal charge on Ir. In valence bond theory, the 3c-4e⁻ bond comprises two ionic resonance structures as shown below. Similar considerations apply to NOsH₃ and (HC)OsH₃; these molecules could be formulated with N≡Os and HC≡Os triple bonds or with double bonds. As shown below, the triple-bonded

(65) Caulton, K. G.; Chisholm, M. H.; Streib, W. E.; Xue, Z. *J. Am. Chem. Soc.* **1991**, *113*, 6082−6090.

(66) Caulton, K. G.; Chisholm, M. H.; Doherty, S.; Folting, K. *Organometallics* **1995**, *14*, 2585−2588.

(67) Ruiz, J.; Vivanco, M.; Floriani, C.; Chiesi-Villa, A.; Guastini, C. *J. Chem. Soc., Chem. Commun.* **1991**, 762−764.

(68) Xue, Z. L.; Li, L. T.; Hoyt, L. K.; Diminnie, J. B.; Pollitte, J. L. *J. Am. Chem. Soc.* **1994**, *116*, 2169−2170.

(69) Li, L. T.; Diminnie, J. B.; Liu, X. Z.; Pollitte, J. L.; Xue, Z. L. *Organometallics* **1996**, *15*, 3520−3527.

Table 4. Computed (DFT(B3LYP) and VALBOND) and Experimental Structures of X=ML₃ Complexes (X = R₂C-, RN-, O-, HC-, N-)

(CH₂)ReH₃	DFT	VALBOND	(NH) ReH₃	DFT	VALBOND	OReH₃	DFT	VALBOND
Re-C	1.83Å	1.77 Å	Re-N	1.72Å	1.68 Å	Re-O	1.67 Å	1.614 Å
Re-H$_A$	1.63Å	1.66 Å	Re-H$_A$	1.62Å	1.66 Å	Re-H$_A$	1.619 Å	1.656 Å
Re-H$_B$	1.66Å	1.65 Å	Re-H$_B$	1.69Å	1.66 Å	Re-H$_B$	1.673 Å	1.652 Å
C-Re-H$_A$	92°	93°	Re-H$_C$	1.66Å	1.65 Å	O-Re-H$_A$	94.0°	92.8°
C-Re-H$_B$	119°	113°	N-Re-H$_A$	92°	92°	O-Re-H$_B$	117.2°	118.4°
H$_A$-Re-H$_B$	98°	108°	N-Re-H$_B$	128°	120°	H$_A$-Re-H$_B$	89.0°	100.0°
H$_B$-Re-H$_B$	119°	119°	N-Re-H$_C$	108°	120°	H$_B$-Re-H$_B$	125.6°	118.0°
H-C-H	118°	117°	H$_A$-Re-H$_B$	87°	79°			
H-C-Re	121°	121°	H$_A$-Re-H$_C$	95°	107°			
			H$_B$-Re-H$_C$	124°	119°			
			H-N-Re	138°	144°			

CH₂TaR₂R'	DFT	VALBOND	X=TaRR'₂	WEYLUH C₃ disorder	VALBOND	CH₂TaH₃	DFT	VALBOND
Ta-CH₂	1.93 Å	1.90 Å	Ta-Si	2.56 Å	2.60 Å	Ta-CH₂	1.90 Å	1.90 Å
Ta-Si	2.66 Å	2.52 Å	Ta-C$_D$	2.21 Å	1.91 Å	Ta-H$_A$	1.76 Å	1.78Å
Ta-Me	2.13 Å	2.16 Å	Ta-C$_S$	2.21 Å	2.18 Å	Ta-H$_B$	1.78 Å	1.77Å
CH₂-Ta-Si	94°	94°	Si-Ta-C$_D$	106°	98°	CH₂-Ta-H$_A$	97°	93°
CH₂-Ta-Me	112°	114°	Si-Ta-C$_S$	106°	97(5)°	CH₂-Ta-H$_B$	109°	113°
H-C-Ta-Me	91°	90°	C$_D$-Ta-C$_S$	113°	116(5)°	H$_A$-Ta-H$_B$	110°	108°
Si-Ta-Me	110°	107°	C$_S$Ta-C$_S$	113°	124°	H$_B$-Ta-H$_B$	118°	119°
Me-Ta-Me	118°	119°	R-C$_D$-Ta-C$_S$	114°	138°	H-C-H	115°	117°
H-C-H	114°	118°	R-C$_D$-Ta-C$_S$	-15°	-19°	H-C-Ta	122°	121°
H-C-Ta	123°	121°	Si-Ta-C$_D$-R	-130°	-128°			

| (CH)OsH₃	DFT	NOsH₃	DFT	VALBOND	(CH)₂IrH₃	DFT
Os-C	1.70 Å	Os-N	1.64 Å	1.73 Å	Ir-C	1.81Å
Os-H$_A$	1.73 Å	Os-H$_A$	1.58 Å	1.68 Å	Ir-H$_A$	1.54Å
Os-H$_B$	1.61 Å	Os-H$_B$	1.66 Å	1.67 Å	Ir-H$_B$	1.64Å
C-Os-H$_A$	118°	N-Os-H$_A$	92°	92°	C-Ir-H$_A$	96°
C-Os-H$_B$	92°	N-Os-H$_B$	112°	120°	C-Ir-H$_B$	106°
C-Os-H$_B$	92°	N-Os-H$_B$	112°	120°	H$_A$-Ir-H$_B$	88°
H$_A$-Os-H$_B$	134°	H$_A$-Os-H$_B$	89°	107°	H$_B$-Ir-H$_B$	148°
H$_A$-Os-H$_B$	134°	H$_A$-Os-H$_B$	89°	77°	H-C-Ir	120°
H$_B$-Os-H$_B$	72°	H$_B$-Os-H$_B$	137°	119°		
H-C-Os	177°					

ª Six-letter Cambridge Structure Database REFCODE citation: WEYLUH.[68]

Table 5. NBO Analyses of X=MH$_3$ Complexes

compound	NPA charges[a]			M σ-bond NBOs[b]		M–X π NBO[c]	X–H/LP NBO[d]	%Lewis density[e]
	M	X	L	M–X	M–L			
H$_2$CReH$_3$	+0.39	−0.14	−0.03	40% Re;sd$^{4.2}$ 60% C;sp$^{1.9}$	48% Re;sd$^{2.4}$ 52% H;s	51% Re 49% C	59% C;sp$^{2.1}$ 41% H	99.8
H$_B$(×2)			−0.11		45% Re;sd$^{2.9}$ 55% H;s			
HNReH$_3$	+0.65	−0.29	0.00	34% Re; sd$^{6.4}$ 66% N; sp$^{3.9}$	50% Re;sd$^{2.0}$ 50% H	37% Re 63% N	68% N;sp$^{3.5}$ 32% H	99.4
H$_B$			−0.23		42% Re;sd$^{2.2}$ 58% H		N LP sp$^{0.8}$	
H$_C$			−0.12		46% Re;sd$^{3.6}$ 54% H			
OReH$_3$	+0.91	−0.49	0.00	29% Re;sd$^{7.2}$ 71% O;sp$^{4.4}$	50% Re;sd$^{1.8}$ 50% H	29% Re 71% O	O LP sp$^{0.2}$ O LP sp$^{1.8}$	99.4
H$_B$(×2)			−0.21		43% Re;sd$^{2.8}$ 57% H			
H$_2$CTaH$_3$	+1.41	−0.49	−0.29	33% Ta; sd$^{3.8}$ 67% C; sp$^{1.8}$	36% Ta;sd$^{2.6}$ 64% H; s	39% Ta 61% C	61% Csp$^{2.1}$ 39% H	99.8
H$_B$(×2)			−0.32		34% Ta; sd$^{2.8}$ 66% H			
H$_2$CIrH$_3$	+0.38	−0.09	+0.12	47% Ir; sd$^{2.8}$ 53% C; sp$^{8.5}$	57% Ir; sd$^{2.2}$ 43% H	46% Ir 54% C	58% C; sp$^{1.9}$ 42% H	98.7
H$_B$(×2)			−0.17		40% Ir; sd$^{2.3}$ 60% H			
NOsH$_3$	+0.62	−0.29	−0.08	43% Os; sd$^{6.4}$ 57% N; sp$^{5.98}$	33% Os; sd$^{0.85}$ 67% H	52% Os 48% N	N LP sp$^{0.2}$	98.9
H$_B$(×2)			−0.20		49% Os; sd$^{2.87}$ 51% H	38% Os 62% N		
HCOsH$_3$	+0.28	+0.05	−0.33	41% Os; sd$^{3.1}$ 59% C; sp$^{0.9}$	32% Os; sd$^{1.0}$ 68% H	62% Os 38% C		98.8
H$_B$(×2)			−0.0		50% Os;sd$^{3.2}$ 50% H	47% Os 53% C		

[a] Atom-centered charges based on natural population analysis (see ref 58). [b] The percent contribution of each atom-centered hybrid to the σ natural bond and the hybrid orbital compositions are given (see ref 58). [c] The percent contribution of the metal-centered d orbital and the ligand-centered p orbital to the π natural bond is given. [d] The composition and hybridization of L−H σ-bond and/or a ligand-centered lone pair. [e] The % of the total electron density that is described by a Lewis structure consisting of core orbitals, bonds, and lone pairs.

structures are formally hypervalent at the Os, whereas the double-bonded structures will have formal charges of −2 and −1 at N and C, respectively. We note that an alternative description of hypervalent compounds, the Bayse−Hall OR-SAM[70] model, is to describe the 3c-4e$^−$ bond as two 2-center−2-electron interactions made from spd combinations.

Normal Valent   Hypervalent Resonance Structures
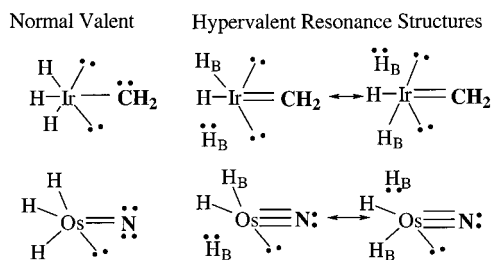
NBO analyses, as well as the geometries, of these Os and Ir complexes corroborate the multiple configuration nature of the electronic structures. Characteristic features of NBO analyses for molecules that cannot be described well with a single-resonance configuration are <99% Lewis density percentages (vs >99.6% for single-configuration cases) and localized orbitals with low (<1.9 electrons) occupancies. As seen in Table 5, (H$_2$C)IrH$_3$, NOsH$_3$, and (HC)OsH$_3$ all have Lewis densities less than 99%. NBO analysis of (H$_2$C)IrH$_3$ finds a double bond but with only 1.6 electrons in the π-bond and 1.71 electrons in the Ir−H$_B$ bonds. Structurally the H$_B$ hydrides are distinguished by a wide H$_B$−Ir−H$_B$ bond angle (148°), significant lengthening

(70) Bayse, C. A.; Hall, M. B. *J. Am. Chem. Soc.* **1999**, *121*, 1348−1358.

of the Ir−H$_B$ bonds (Ir−H$_B$ is longer than Ir−H$_A$ by 0.1 Å), an accumulation of negative charge H$_B$ (each H$_B$ has −0.17 charge as compared with +0.12 charge on H$_A$). Thus, for (H$_2$C)IrH$_3$ the double-bonded "hypervalent" structure dominates, but not completely.

NOsH$_3$ and (HC)OsH$_3$ both show partial occupancies (1.7 electrons) of just one of the two localized π-bonds. As a result, the X-Os linkage has a bond order between 2 and 3, and C_3 symmetry is not enforced. In both complexes the Os−H bonds which are perpendicular to the X−Os axis are apolar, and the other Os−H bonds are polarized toward H. Interestingly, in (HC)OsH$_3$ there is just one polarized Os−H bond (Os−H$_A$), suggesting the primary resonance delocalization involves a lone pair on C in hyperconjugation with the Os−H$_A$ σ-bond.
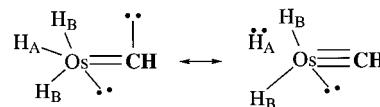
Singly-Bonded X−MH$_3$: OIrH$_3$. According to our prescriptions, OIrH$_3$ has an O−Ir single bond, formal charges of +1 (Ir) and −1 (O), and two lone pairs on Ir. The bond hybridizations are sd^3, and an approximate tetrahedral coordination geometry is expected. The DFT(B3LYP)-computed minimum (Table 6) has O−Ir−H bond angles of 116° and H−Ir−H bond angles of 102°; such distortion from an idealized tetrahedron is expected due to the high polarity of the Ir−O bond. Although the DFT(B3LYP)-optimized structures of both NWH$_3$ and OIrH$_3$ have C_{3v} point group symmetries, the bonding clearly is different as revealed by the X−M−H bond angles which are close to 90° for the W complex and 116° for the Ir complex.

Table 6. Computed (DFT(B3LYP) and VALBOND) and Experimental Geometries of OIrL₃ Complexes

OIrMe₃	DFT	VALBOND	OIrH₃	DFT	VALBOND	OIr(Mesityl)₃	HEDNUZ[a]	VALBOND
Ir–O	1.76 Å	1.79 Å	Ir–O	1.72 Å	1.79 Å	Ir–O	1.73 Å	1.66 Å
Ir–Me	2.05 Å	1.96 Å	Ir–H	1.58 Å	1.59 Å	Ir–L₁	2.02(2) Å	1.96 Å
O–Ir–Me	116°	111°	O–Ir–H	116°	112°	O–Ir–L₁	111(6)°	106°
Me–Ir–Me	102°	108°	H–Ir–H	102°	107°	L₁–Ir–L₂	109(6)°	112°

[a] Six-letter Cambridge Structure Database REFCODE citation: HEDNUZ.[71]

Although consistent with the predominance of the O–Ir single-bonded structure, NBO analysis of OIrH₃ indicates some hyperconjugation of O lone pairs with the Ir–H σ-bonds. Charges of $+0.74$ at Ir, -0.65 at O, and -0.03 at each of the H's are found. The Ir–H bonds are relatively apolar (53% Ir/ 47% H) and have sd$^{2.4}$ hybridization. In contrast the O–Ir bond is more polar (41% Ir/59% O) and high in Ir d-character (sd$^{7.8}$) and O p-character (sp$^{10.4}$). The participation of O=Ir double-bonded structures is indicated by the moderately low Lewis percentage (99.2%) and partial occupation of the two pure pπ lone pairs on the O (1.7 electrons) with delocalization (0.2 electrons) into the three Ir–H antibonds. *Overall, OIrH₃ is the transition metal analogue of a phosphine oxide (OPR₃).* Accordingly the O–Ir bonds are short (1.72 Å), highly polar, single bonds with some hyperconjugation of the O pπ lone pairs. VALBOND computations, which are based on a single configuration containing a O–Ir single bond, yield a sterling reproduction of the crystallographic shape of OIr(mesityl)₃.[71]

H₃MMH₃: Computed Structures. In principle, the valence bond model provides simple prescriptions for Lewis-like structures containing metal–metal σ- and π-bonds. By direct analogy with previous examples and in accordance with the Lewis structures shown below we anticipate that the complexes H₃WWH₃, H₃ReReH₃, and H₃OsOsH₃ will contain triple, double, and single bonds with the following molecular shapes: triply bonded H₃WWH₃ should exhibit three-fold symmetry with near 90° H–W–W bond angles (similar to HCWH₃), doubly bonded H₃ReReH₃ should exhibit low symmetry (C_s or C_1) with near 90° H–Re–Re bond angles for H's that lie in the plane of the Re–Re dπ–dπ bond and larger angles for the other H's (similar to H₂CReH₃), and singly bonded H₃OsOsH₃ should exhibit three-fold symmetry with H–Os–Os bond angles near 110° (similar to OsH₄). We were delighted to find that both DFT(B3LYP) computations and VALBOND computations minimized to the anticipated molecular shapes.

The DFT(B3LYP)- and VALBOND-optimized structures for H₃WWH₃, H₃ReReH₃, and H₃OsOsH₃ are presented in Table 7. These shapes about the transition metal atoms are strikingly similar to those of X≡WH₃, X=ReH₃, and X–OsH₃ complexes. NBO analysis of the DFT(B3LYP) density conforms to a simple Lewis description featuring localized metal–metal triple, double,

and single bonds about sd³-hybridized σ-bonding frameworks. Thus, metal–metal bonding can, at least in these instances, be described efficiently and usefully with hybridized, localized bonds.

XMH₄ Complexes: Computed and Experimental Structures. As we have shown in the previous sections, metal–ligand π-bonding has profound effects on molecular shapes. These effects can be understood using a localized bond framework. In the VB-like model, minimization of bond-overlaps involving both the σ- and π-bond frameworks determines the observed geometry. The analysis of XML₄ complexes follows similar reasoning. Previously, Kaupp[48] has analyzed distortions in some OML₄ complexes from a molecular orbital perspective. Ward also has examined the general structures of MX₂L₃ complexes.[72] Our analysis provides a valence bond perspective.

Let us begin with the hypothetical compounds, (H₂C)WH₄ and OWH₄. The pure σ-bonded reference compound is sd⁴-hybridized WH₅⁺, which we have previously shown adopts a DFT(B3LYP)-minimized square pyramidal geometry.[18] However, the potential energy surface of WH₅⁺ is complicated and has multiple local minima. Previously, we have suggested that *multiple minima arise because there is no single geometry that can accommodate the 66° and 114° bond angle preferences of sd⁴ hybrid orbitals.* With the addition of a π-bond to the sd⁴-hybridized σ-bonding we anticipate near 90° bond angles for hydrogens that lie in the plane of the dπ-bond, and bond angles closer to 66° and 114° for hydrogens that lie in the plane orthogonal to the lobes of the dπ-bond.

X=ML₄ Complexes. The simple alkylidene, H₂C=WH₄, provides a clean computational model of a metal with one localized π-bond to a ligand. As shown in Table 8 the DFT-(B3LYP)-computed structure of H₂CWH₄ is significantly distorted from the square pyramidal minimum of WH₅⁺. The primary distortion is the movement of the two hydrides, H_c, that are most nearly coplanar with the lobes of the dπ W orbital to form C–W–H bond angles close to 90°. This movement minimizes overlap of the W–H σ-bonds with the dπ orbital. From a structural viewpoint, the compounds O=WH₄ and HN= WH₄ are quite similar to the alkylidene, H₂C=WH₄. The primary differences between these structures are slight changes in the X–W–H_c angles. Thus, again we see clear indication of

(71) Hay-Motherwell, R. S.; Wilkinson, G.; Hussain-Bates, B.; Hursthouse, M. B. *Polyhedron* **1993**, *12*, 2009–2012.

(72) Ward, T. R.; Burgi, H. B.; Gilardoni, P.; Weber, J. *J. Am. Chem. Soc.* **1997**, *119*, 11974–11985.

Table 7. VALBOND and DFT(B3LYP) Optimized Geometries of H_3MMH_3 complexes (M=W,Re, Os)

H_3WWH_3	DFT	VALBOND	H_3ReReH_3	DFT	VALBOND	H_3OsOsH_3	DFT	VALBOND
W-W	2.24 Å	2.28 Å	Re-Re	2.21 Å	2.36 Å	Os-Os	2.34 Å	2.32 Å
W-H	1.72 Å	1.67 Å	Re-H	1.64 Å	1.66 Å	Os-H	1.61 Å	1.54 Å
H-W-H	120°	120°	Re-H_B	1.68 Å	1.66 Å	H-Os-H	110°	110°
H-W-W	94°	90°	H_A-Re-H_B	108°	117°	H-Os-Os	109°	109°
H-W-W-H	60°	60°	H_B-Re-H_B	128°	117°	H-Os-Os-H	±60°	±60°
	180°	180°					180°	180°
			H_A-Re-Re	91°	93°			
			H_B-Re-Re	107°	113°			
			H_A-Re-Re-H_B	±71°	±62			
			H_A-Re-Re-H_A	180°	180°			

Table 8. Computed (DFT(B3LYP) and VALBOND) Geometries of X=WH$_4$ Complexes

$(CH_2)WH_4$	DFT	VALBOND	$(NH)WH_4$	DFT	VALBOND	OWH_4	DFT	VALBOND
W-C	1.87 Å	1.84 Å	W-N	1.73 Å	1.74 Å	W-O	1.69 Å	1.68 Å
W-H_A	1.74 Å	1.72 Å	W-H_A	1.76 Å	1.72 Å	W-H_A	1.76 Å	1.72 Å
W-H_B	1.68 Å	1.74 Å	W-H_B	1.72 Å	1.73 Å	W-H_B	1.70 Å	1.73 Å
W-H_C	1.69 Å	1.73 Å	W-H_C	1.69 Å	1.73 Å	W-H_C	1.68 Å	1.73 Å
C-W-H_A	115°	119°	N-W-H_A	112°	120°	O-W-H_A	118°	120°
C-W-H_B	122°	122°	N-W-H_B	114°	122°	O-W-H_B	110°	123°
C-W-H_C	94°	90°	N-W-H_C	97°	89°	O-W-H_C	99°	89°
H_A-W-H_B	123°	119°	H_A-W-H_B	133°	118°	H_A-W-H_B	132°	117°
H_B-W-H_C	65°	65°	H_A-W-H_C	112°	116°	H_A-W-H_C	110°	116°
H_C-W-H_C	125°	121°	H_B-W-H_C	62°	66°	H_B-W-H_C	60°	66°
H-C-H	117°	117°	H_C-W-H_C	122°	121°	H_C-W-H_C	120°	121°
H-C-W	121(9)°	121°	H-N-W	161°	144°			

a single localized π-bond even in an oxo compound that has no other symmetry-lowering attachments. Further support for the simple Lewis-like description of the bonding in X=ML$_4$ complexes is provided by VALBOND computations. VAL-BOND computations reproduce the DFT(B3LYP) results quite well. As we have seen before, the unoptimized VALBOND parameters overemphasize nonorthogonalities involving the π-bonds, leading to X−M−H$_c$ angles that are slightly closer to 90°.

The NBO analyses (Table 9) of X=WH$_4$ compounds generally conform to the Lewis structures prescribed by our rules. Thus, the dominant resonance structure contains an X=W double bond and four W−H σ-bonds. As expected, the average

W−H hybridization is slightly lower than sd^4 due to the polarity of the X−W bonds.

X−ML$_4$ Complexes. According to the Lewis-like model, complexes with the formula XOsH$_4$ (X=H$_2$C−,HN−, and O−) will either contain X−Os single bonds (normal valent) or have X=Os and be hypervalent. The overall shapes of the metal complexes shed light on the bonding, albeit with some reservations due to the general softness of the sd^4-hybridized σ-bond framework. An X−Os single bond is expected to yield a square pyramidal structure in keeping with approximate sd^4 hybridization among five σ-bonds, whereas significant X=Os double bond character should render a lower-symmetry structure similar to those found for XWH$_4$ complexes.

Table 9. NBO Analyses of X=MH$_4$ Complexes

compound	NPA charges[a]			π-bond NBOs[b]		M−X π NBO[c]	X−H/LP NBO[d]	%Lewis density[e]
	M	X	H	M−X	M−H			
H$_2$CWH$_4$	+0.72	−0.26	−0.21	37% W; sd$^{4.3}$	48% W; sd$^{5.3}$	48% W	59% C; sp$^{2.3}$	99.6
				63% C; sp$^{1.8}$	52% H; s	52% C	41% H	
H$_B$			−0.06		40% W; sd$^{3.2}$		60% C; sp$^{2.0}$	
					60% H; s		40% H	
H$_C$(×2)			−0.09		45% W; sd$^{3.8}$			
					55% H; s			
HNWH$_4$	+1.0	−0.38	−0.29	29% W; sd$^{7.4}$	45% W; sd$^{3.5}$	33% W	70% N; sp$^{2.7}$	99.0
				71% N; sp$^{2.7}$	55% H	67% N	30% H	
H$_B$			−0.14		38% W; sd$^{4.9}$		N LP sp$^{1.2}$	
					62% H			
H$_C$(×2)			−0.09		42% W; sd$^{3.03}$			
					58% H			
OWH$_4$	+1.2	−0.6	−0.32	29% W; sd$^{7.2}$	37% W; sd$^{2.5}$	25% W	O LP sp$^{0.2}$	99.2
				71% O; sp$^{3.9}$	63% H	75% O	O LP pure p	
H$_B$			−0.10		48% W; sd$^{6.6}$			
					52% H			
H$_C$(×2)			−0.09		46% W; sd$^{3.3}$			
					54% H			
OOsH$_4$	+0.76	−0.55	−0.05	35% Os; sd$^{9.9}$	52% Os; sd$^{3.4}$	39% Os	O LP sp$^{0.2}$	98.9
				65% O; sp$^{6.1}$	48% H; s	61% O	O LP pure p	
							(×2)	

[a] Atom-centered charges based on natural population analysis (see ref 58). [b] The percent contribution of each atom-centered hybrid to the σ natural bond and the hybrid orbital compositions are given (see ref 58). [c] The percent contribution of the metal-centered d orbital and the ligand-centered p orbital to the π natural bond is given. [d] The composition and hybridization of L−H σ-bond and/or a ligand-centered lone pair. [e] The percentage of the total electron density that is described by a Lewis structure consisting of core orbitals, bonds, and lone pairs.

The X−Os bond character varies from a nominal single bond (OOsH$_4$) to double bond (H$_2$COsH$_4$) as the electronegativity of X decreases, with the imido complex between the two limits. Consistent with an O−Os single bond formulation is the geometry (square pyramidal with O−Os−H and H−Os−H bond angles close to those of WH$_5^+$) and the NBO analysis (a very polar single Os−O σ-bond, sd$^{3.4}$ hybridization of the Os−H σ-bonds), Again, however, we see indications of hyperconjugation of the O lone pairs with the Os−H bonds (1.6 electron occupation of the pπ O lone pairs, 0.2 electron occupation of the Os−H antibonds). Although the VALBOND computations do not take these delocalizations into account, the overall fit between the VALBOND and DFT(B3LYP) geometries is very good (Table 10).

Characteristics of the imido and alkylidene complexes that suggest higher X−Os bond orders include the geometries (low symmetry, C_s, about the Os, planarity at the alkylidene C, extensive asymmetry in the Os−H bond lengths of H$_2$COsH$_4$, and a bent H−N−Os angle) and NBO analyses (X=Os double bonds) which are not presented. However, it should be emphasized that the NBO analyses show strong characteristics of structures that are not well described by just one resonance structure (ca. 98.5% Lewis character, partial occupancies of the X−Os π-bond and Os−H bonds).

VALBOND computations of X−ML$_4$ structures containing X−M single bonds give remarkably good agreement with DFT-(B3LYP) computations and crystallographically determined structures as shown in Table 10. These computations include a number of systems that are isoelectronic with OOsH$_4$ ([ORe(CH$_2$TMS)$_4$]$^-$,[73] OOs(CH$_2$TMS)$_4$,[74] OOs(CH$_3$)$_4$, [NOs(CH$_2$TMS)$_4$]$^-$,[75] HNOs(CH$_3$)$_4$, MeNOs(CH$_2$TMS)$_4$).[75] Also included are radicals with one fewer electron than OOsL$_4$ (ORe-

(o-tolyl)$_4$,[76] ORe(mesityl)$_4$,[77] ORe(methyl)$_4$, OW(o-xylyl)$_2$);[78] by our prescriptions these complexes differ from OOsL$_4$ only by singly, rather than doubly, occupying a nonbonding Os d orbital.

X$_2$ML$_2$ Complexes: Computed and Experimental Geometries. Given the remarkable impact of even a single metal−ligand π-bond on the geometry of transition metal complexes, it is interesting to examine complexes with π-bonds to two or more ligands. In addition to the effects of π-bonding on geometry that we have already seen (i.e., the final geometries represent a compromise between minimization of σ−σ and σ−π overlaps), complexes with two π-bonds will exhibit the added effect of minimizing π−π overlaps. For dioxo and diimido X$_2$-ML$_2$ cases, one anticipates greater ionic character in the overall bonding than seen for the monooxo and monoimido cases. This should result in greater deviation of the observed geometries from those prescribed by a covalent, Lewis-like picture.

The DFT(B3LYP)-computed structures (Table 11) of the diimido and dioxo X$_2$WH$_2$ complexes differ significantly from the alkylidene structure and from the VALBOND computations. Strong support for the bonding model, and validation of the "balance-of-forces" approach to rationalizing structures, is found in the alkylidene, (H$_2$C)$_2$WH$_2$, structural features (low symmetry, 95° H$_A$−W−C bond angles for the hydride that lies in the plane of the W−C π-bond, nearly coplanar orientations of the two H$_2$C−W planes, and excellent agreement between crystallographic and VALBOND structures) and NBO metrics (two W=C double bonds, 99.6% Lewis character, high orbital occupancies). Note that the unobtainable, idealized structural preferences are 109° bond angles for σ-bond framework, 90° for the π-bond framework, and either 0° or 90° angles between

(73) Stavropoulos, P.; Edwards, P. G.; Wilkinson, G.; Motevalli, M.; Malik, K. M. A.; Hursthouse, M. B. *J. Chem. Soc., Dalton Trans.* **1985**, 2167−2175.

(74) Marshman, R. W.; Bigham, W. S.; Wilson, S. R.; Shapley, P. A. *Organometallics* **1990**, *9*, 1341−1343.

(75) Shapley, P. A.; Kim, H. S.; Wilson, S. R. *Organometallics* **1988**, *7*, 928−933.

(76) Savage, P. D.; Wilkinson, G.; Motevalli, M.; Hursthouse, M. B. *J. Chem. Soc., Dalton Trans.* **1988**, 669−673.

(77) Stavropoulos, P.; Edwards, P. G.; Behling, T.; Wilkinson, G.; Motevalli, M.; Hursthouse, M. B. *J. Chem. Soc., Dalton Trans.* **1987**, 169−175.

(78) Lappert, M. F.; Raston, C. L.; Rowbottom, G. L.; White, A. H. *J. Chem. Soc., Chem. Commun.* **1981**, 6−8.

Table 10. Computed (DFT(B3LYP) and VALBOND) and Experimental Geometries of XML$_4$ Complexes

(CH)$_2$OsH$_4$	DFT	(NH)OsH$_4$	DFT	VALBOND	OOsH$_4$	DFT	VALBOND
Os-C	1.82Å	Os-N	1.73 Å	1.92 Å	Os-O	1.68 Å	1.87 Å
Os-H$_A$	1.66Å	Os-H$_A$	1.62 Å	1.68 Å	Os-H	1.62 Å	1.68 Å
Os-H$_B$	1.60Å	Os-H$_B$	1.63 Å	1.68 Å	O-Os-H	116°	120°
C-Os-H$_A$	105°	N-Os-H$_A$	106°	118°			
C-Os-H$_B$	106°	N-Os-H$_B$	124°	117°			
H$_A$-Os-H$_B$	68°	H$_A$-Os-H$_B$	73°	66°	H-Os-H	79°	75°
	127°		128°	118°		127°	118°
H$_B$-Os-H$_B$	62°	H$_B$-Os-H$_B$	109°	110°			
H$_A$-Os-H$_A$	139°	H$_A$-Os-H$_A$	68°	64°			
Os-C-H	121(9)°	Os-N-H	134°	138°			
H-C-H	118°						

OReMe$_4$	DFT	VALBOND	OOsR$_4$ R=CH$_2$TMS	VESJEI[a]	VALBOND
Re-O	1.72Å	1.85Å	Os-O	1.69 Å	1.96 Å
Re-Me	2.13Å	2.06Å	Os-R	2.10(3)Å	2.10 Å
O-Re-Me	112°	118°	O-Os-R	112(6)°	118(2)°
Me-Re-Me	82°	77°	R-Os-R	83(2)°	77(1)°
	135°	124°		140(12)°	125(3)°

[NOsMe$_4$]$^-$	DFT	VALBOND	[NOsR$_4$]$^-$ R=CH$_2$TMS	DULMAY	VALBOND
Os-N	1.68 Å	1.98 Å	Os-N	1.63 Å	1.98 Å
Os-Me	2.15 Å	2.08 Å	Os-R	2.13(2)Å	2.09(1)Å
N-Os-Me	110°	119°	N-Os-R	108(1)°	118(1)°
Me-Os-Me	84°	77°	R-Os-R	84(1)°	77(1)°
	141°	123°		145°	125°

[a] Six-letter Cambridge Database REFCODE citations: VESJEI,[74] DULMAY.[75]

the two alkylidene planes due to minimization of π−π overlap. As expected, VALBOND computations on the diimido and dioxo X$_2$WH$_2$ complexes yield symmetry-broken structures similar to those of (H$_2$C)$_2$WH$_2$. However, the DFT(B3LYP)-computed geometries exhibit C_{2v} symmetry, and NBO analysis of the DFT(B3LYP) electron density indicates the need for multiple resonance structures: high charges at the W (+1.4 for

X=HN and +1.7 for X=O), low-occupancy and highly polarized X≡W "triple bonds", strong delocalizations (mainly hyperconjugation involving W−H bonds and X−W antibonds), and low %Lewis densities (98.6% for X=HN and 98.8% for X=O). It is not surprising that the dioxo and diimido complexes are more ionic and, hence, require different "rules" for creating appropriate Lewis structures.

Table 11. VALBOND and DFT(B3LYP) Computed Geometries of (X=)$_2$WL$_2$ complexes
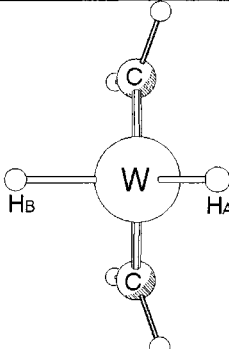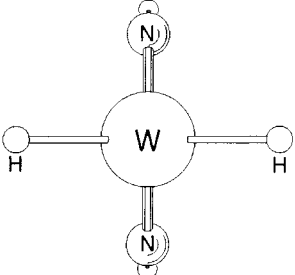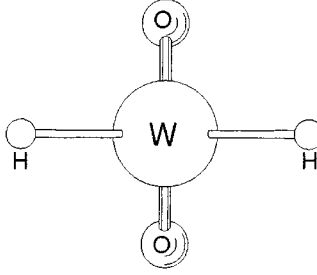

(CH$_2$)$_2$WH$_2$	DFT	VALBOND	(NH)$_2$WH$_2$	DFT	VALBOND	O$_2$WH$_2$	DFT	VALBOND
W-C	1.88 Å	1.84 Å	W-N	1.75 Å	1.74 Å	W-O	1.71 Å	1.68 Å
W-H$_A$	1.74 Å	1.73 Å	W-H$_A$	1.73 Å	1.73 Å	W-H$_A$	1.72 Å	1.72 Å
W-H$_B$	1.70 Å	1.72 Å	W-H$_B$	1.73 Å	1.72 Å	W-H$_B$	1.72 Å	1.73 Å
C-W-C	110°	106°	N-W-N	114°	107°	O-W-O	110°	107°
C-W-H$_A$	120°	122°	N-W-H$_A$	105°	122°	O-W-H$_A$	107°	122°
H-C-W-H$_A$	16°	6°	H-N-W-H$_A$	-115°	174°	O-W-H$_B$	107°	93°
C-W-H$_B$	96°	93°	N-W-H$_B$	105°	93°	H$_A$-W-H$_B$	119°	111°
H$_A$-W-H$_B$	111°	113°	H-N-W-H$_B$	115°	-69°			
H-C-H	116°	117°	H$_A$-W-H$_B$	122°	111°			
H-C-W	122(4)°	121°	H-N-W	153°	144°			

Table 12. Computed (DFT(B3LYP) and VALBOND) and Experimental Geometries of (X=)$_2$ML$_2$ Complexes

(HN)$_2$MoMe$_2$	DFT	VALBOND	(t-BuN)$_2$Mo(R)$_2$	FUNNAD[a]	VALBOND
Mo-N	1.76 Å	1.70 Å	Mo-N	1.72(1)Å	1.70 Å
Mo-C	2.12 Å	2.04 Å	Mo-C	2.16 Å	2.05 Å
N-Mo-N	114°	106°	N-Mo-N	112°	98°
C-Mo-C	116°	111°	C-Mo-C	123°	116°
N-Mo-C	107°	122°	N-Mo-C	106(3)°	108(10)°
H-N-Mo	156°	144°	Mo-N-C	161°	152(2)°
H-N-Mo-N	0°	141°			
H-N-Mo-C	-118°	6°			

[a] Six-letter Cambridge Database REFCODE citation: FUNNAD.[79]

Because of the shortcomings of the single-configuration description of (RN)$_2$ML$_2$ structures, the VALBOND optimizations of a series of crystallographically characterized diimido dialkyl complexes (bis(*tert*-butylimido)bis(mesityl)chromium,[79] bis(2,6-diisopropylphenylimido)bis(neopentyl)chromium,[80] bis-(*tert*-butylimido)bis(mesityl)molybdenum,[79] and bis(2,6-diisopropylphenylimido)bis(neopentyl)molybdenum[81]) exhibit systematic deviations from experiment. As seen with the simple hydrides, the VALBOND computations yield RN−W−R′ bond angles that are symmetry-broken with one angle tending toward 90° and the other tending toward 120°, whereas the crystallographic structures reveal average RN−W−R′ angles around 109° (see Table 12).

Conclusions

The presence of metal−ligand π-bonding strongly influences the shapes of transition metal complexes. Our approach to understanding the shapes of transition metal complexes with metal−ligand π-bonding emphasizes a VB perspective: we highlight the primary role of the metal s and d orbital hybridization in forming localized metal−ligand σ-bonds, the special role of the 12-electron count at metal centers, and the structural consequences of the balance of forces arising from overlap of $\sigma-\sigma$, $\sigma-\pi$, and $\pi-\pi$ localized orbitals. For structures that are not well-described by a single Lewis structure, concepts such as formal charges, hypervalence, hyperconjugation, and ionic resonance extend the bonding model.

Although unconventional, the VB-like model of transition metal complexes containing metal−ligand or metal−metal multiple bonds is reasonable, useful, and significant. The reasonableness of this strategy is illustrated by the consistency of the Lewis-like structures with detailed analysis of ab initio electron density distributions as determined either from NBO analyses or by comparison with the resonance structure analyses of Cundari and Gordon.[25] Utility is demonstrated by the effectiveness of molecular mechanics algorithms which are derived from VB-like considerations. The significance of this work is that it (1) provides a localized bond "connection" between the p-block and d-block that emphasizes a consistent Lewis-like formulation, (2) contributes an easily applied set of bonding principles for understanding the large perturbations in molecular shapes that accompany changes in electron count and π-bond orders, and (3) represents the first molecular mechanics method capable of describing non-"points-on-a-sphere" shapes[12] of organometallic complexes containing metal−ligand π-bonds.

The model that we have described is limited, at least in its current form, to complexes that are dominated by covalent bonding. It is not surprising that a VB-like model does not provide a good zeroth-order description of the bonding when the structure contains strong ionic contributions. In the spirit of a VB-like model, the incorporation of ionic-bonding effects suggests the inclusion of multiple resonance structures. Our future work will be aimed at creating simple rules for generating appropriate resonance configurations and algorithms for assessing their influence on molecular structure and energetics.

(79) Sullivan, A. C.; Wilkinson, G.; Motevalli, M.; Hursthouse, M. B. *J. Chem. Soc., Dalton Trans.* **1988**, 53−60.

(80) Coles, M. P.; Gibson, V. L.; Clegg, W.; Elsegood, M. R. J.; Porrelli, P. A. *J. Chem. Soc., Chem. Commun.* **1996**, 1963−1964.

(81) Bell, A.; Clegg, W.; Dyer, P. W.; Elsegood, M. R. J.; Gibson, V. L.; Marshall, E. *J. Chem. Soc., Chem. Commun.* **1994**, 2547−2548.

Computational Methods

A. Electronic Structure Calculations. The density functional theory (DFT) method B3LYP[82,83] was used throughout for electronic structure calculations. The Jaguar program[84] was used to model all structures. The core electrons of transition metal atoms were simulated with an effective core potential. The valence and underlying shell of electrons were described explicitly with a triple-ζ contraction based on the basis set developed by Hay and Wadt[85] for metals and a 6-311++G** basis for main group elements. As in our earlier work, extensive conformational searching was employed to mitigate problems with multiple local minima. In general, the starting conformations were taken from local minima previously found for hydrides with similar σ-bond hybridizations. Each structure was found to be a local energy minimum by calculation of its vibrational frequencies.

To analyze localized population densities, we use natural bond orbital (NBO) analysis.[59] NBO generates localized bonding structures, which are usually identical or similar to the resonance structures we use for molecular modeling. We have found that those compounds for which NBO gives clean, localized structures are well-described by our MM algorithm. On the other hand, compounds with electronic density not well localized by NBO are often poorly described by a single resonance structure in VALBOND.

B. Molecular Mechanics Computations. The MM program, VALBOND, is a modified version of the UFF2[86] program. In short, the total energy is expressed according to the following sum:

$$E_{tot} = E_{bond} + E_{angle} + E_{torsion} + E_{improper} + E_{electrostatic} + E_{VDW}$$

A full listing of the UFF potential energy functions and parameters is provided as Supporting Information. For computations in this paper, no electrostatic contributions to the total energy were computed. The UFF/VALBOND force field is a rule-based molecular mechanics program with minimal parametrization. Because the purpose of using molecular mechanics computations in this paper is the testing of general bonding concepts, we consistently have resisted the temptation to adjust parameters to better fit ab initio and experimental structures. Accordingly, default values of parameters are used throughout.

VALBOND Angular Terms. The VALBOND version of the program replaces the angular potential energy functions with algorithms based on hybrid orbital overlaps as has been described in detail previously.[18] We have slightly modified the previously used VALBOND functions as follows. The overlap (Δ) of two hybrid orbitals centered on the same atom and making σ-bonds to ligand 1 and ligand 2 is given in eq 1, where α is the ligand−metal−ligand angle and m_1, n_1, m_2, and n_2 are the hybridization coefficients in the standard form ($sp^{m1}d^{n1}$ and $sp^{m2}d^{n2}$) for the two σ hybrid orbitals. Equations 2 and 3 are unchanged from the previous VALBOND routines: St(α) is the "strength function" as defined by Pauling, and S^{max} is the maximum value of the "strength function" for a given hybridization. The molecular mechanics potential energy function is given by eq 4, which is identical to the previous form of the VALBOND equations.

$$\Delta = \frac{1 + \sqrt{m_1 m_2}\cos\alpha + \sqrt{n_1 n_2}\dfrac{(3\cos^2\alpha - 1)}{2}}{\sqrt{1 + m_1 + n_1}\sqrt{1 + m_2 + n_2}} \quad (1)$$

$$S^{max_1} = \sqrt{\frac{1}{1 + m_1 + n_1}}(1 + \sqrt{3}m_1 + \sqrt{5}n_1) \quad (2)$$

$$St(\alpha) = \sqrt{1 - \frac{1 - \sqrt{(1 - \Delta^2)}}{2}} \quad (3)$$

$$E(\alpha) = (1 - St(\alpha))(S^{max_1}k1 + S^{max_2}k2) \quad (4)$$

This newer algorithm[87] is identical to the previous algorithm when all of the ligands bonded to the central atom are identical. For nonhomoleptic complexes (i.e., those with dissimilar ligands), the advantage of the newer algorithm is that it yields zero angular potential energy at the minimum, whereas the previous algorithm always yielded slightly positive values. The newer and older algorithms give very similar molecular geometries.

VALBOND Treatment of π-Bonds. The construction of potential energy functions for π-bonds requires consideration of (1) the distance between the π-bonding atoms, (2) the angular components of the overlap of the π-bond forming orbitals and (3) the overlap of the metal-centered π-bonding orbital with the other σ- and π-bonding orbitals on the metal center. Consider a metal−ligand (M−L) double bond comprising one σ-bond and one π-bond. The M−L bond stretch potential energy is modeled with the extended Rydberg function that is standard to UFF2 and given in Supporting Information. An M−L double bond is assigned a bond order of 2. The equilibrium bond distance for the M−L double bond is determined from default covalent radii for the bonded atoms combined with bond order and electronegativity corrections. The M−L bond dissociation energy is based on bond-order corrected arithmetic averages of default M−M and L−L single bond energies. All of these formula and parameters are standard to UFF2 and are provided as Supporting Information.

Description of the orbital angular overlaps associated with M−L π-bonds within a molecular mechanics framework requires the addition of pseudoatoms. Unlike σ-bonding hybrids, the overlap of a metal dπ and ligand dπ orbital depends on the coplanarity of the two π orbitals as well as the distance betwee M and L. In VALBOND, we measure the coplanarity of the π-bonding orbitals by creating a special dihedral angle term. Special pseudoatoms, called π-pseudoatoms (PI), are attached to M and L in order to create the dihedral angle topology. These pseudoatoms are massless, volumeless points that are attached to their central atoms at a fixed distance by bonds with high force constants. There are no van der Waals energies, electrostatic energies, or bond energies associated with the pseudoatoms. As shown below, when the dihedral angle is 0° or 180°, the π-bonding atomic orbitals are coplanar. Dihedral angles of 90° or 270° indicate zero overlap of the π-bonding atomic orbitals.

Maximum Overlap
PI-L-M-PI = 0°, 180°

Minimum Overlap
PI-L-M-PI = 90°, -90°
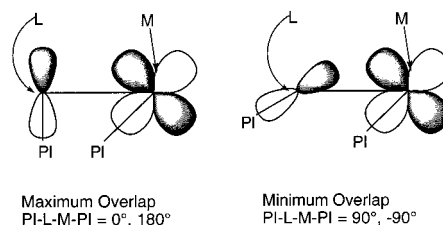
Standard molecular mechanics processing of the PI−L−M−PI topology creates two types of potential energy terms: a torsion energy term ($E_{t\pi}$) that represents the energy of a π-bond as a function of the PI−L−M−PI torsion angle (ϕ) and the distance (r_m) and two bond angle terms that represent the potential energy due to overlap of the π-hybrid orbitals with other hybrid orbitals centered on those atoms based on eq 4.

The expression for the $E_{t\pi}$ term is given below; which is based on our previous description of the π-bond in ethylene.[55,80]

$$E_{t\pi} =$$
$$-260 \text{ kcal/mol} \cdot \cos^2\phi \cdot e^{-2r_m}(1 + 2r_m(1 + 0.3r_m(1 + 0.3r_m))) \times$$
$$(2 \cdot (bo2 - 1)) \quad (5)$$

$r_m = 1.67*$ distance between the central two atoms of the torsion, and bo2 is the bond order for the L−M bond (2 or 3)

This energy term has a minima at $\phi = 0°$, 180° and a maxima at $\phi = 90°$, 270° due to the $\cos^2\phi$ component. The term -260 kcal/mol $\cdot e^{-2r_m}(1 + 2r_m(1 + 0.3r_m(1 + 0.3r_m)))$ provides energy-lowering as the π-bond is shortened. The factors of 1.67 and -260 kcal/mol were

(82) Becke, A. D. *Phys. Rev. A* **1988**, *38*, 3098.
(83) Lee, C.; Yang, W.; Parr, R. G. *Phys. Rev. B* **1988**, *37*, 785−789.
(84) *Jaguar 3.5*; Schödinger, Inc.: Portland, OR, 1998.
(85) Hay, P. J.; Wadt, W. R. *J. Chem. Phys.* **1985**, *82*, 299.
(86) Rappè, A. K.; Pietsch, M. A.; Wiser, D. C.; Hart, J. R.; Bormann, L. M.; Skiff, W. M. *Mol. Eng.* **1997**, *7*, 385−400.
(87) Root, D. M. Ph.D. Thesis; University of Wisconsin: Madison, 1997.

determined empirically from the potential energy surfaces for homolytic cleavage of the ethylene π-bond. In that modeling, it was shown that the VALBOND force field gives an excellent fit to the GVB-RCI potential energy surface for the homolytic cleavage of ethylene into two triplet methylene fragments.[55,80] These default values lead to an overestimate of metal−ligand π-bond strength which, in turn, results in M=L and M≡L bond lengths that are modestly shorter than ab initio and experimental values.

An angular term describes the loss of bonding as the idealized M $d\pi$ orbital of a π-bond loses orthogonality with an idealized sd^n-hybridized σ-hybrid at M. The energy associated with this loss of orthogonality is given by eq 4; the problem is computing the overlap. The computation of the overlap between an sd^n σ-hybrid and a $d\pi$ orbital at a metal center as a function of the angle between the orbitals is simplified by recognizing that the cloverleaf shape of a $d\pi$ orbital (e.g., the $d_{x^2-y^2}$) can be constructed from a linear combination of two orbitals (e.g., the "d_{x^2}" = $d_{2x^2-y^2-z^2}$ and d_{y^2} = $d_{2y^2-x^2-z^2}$) with the shape of a d_{z^2} orbital.
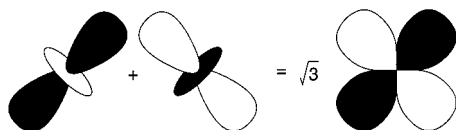
The overlap of a σ-bond to one of the above component orbitals depends on the angle they form, as in eq 1 above where the angle formed was α. There are two components to consider in this case, resulting in dependence on two angles, which we label α and β. The overlap (Δ) between a $d\pi$ orbital and a sd^n-hybridized σ-bond formulated as follows:

$$\Delta = \frac{\sqrt{n}\left[\left(3\cos^2\alpha - 1\right) - \left(3\cos^2\beta - 1\right)\right]}{2\sqrt{3}\sqrt{1+n}} \tag{6}$$
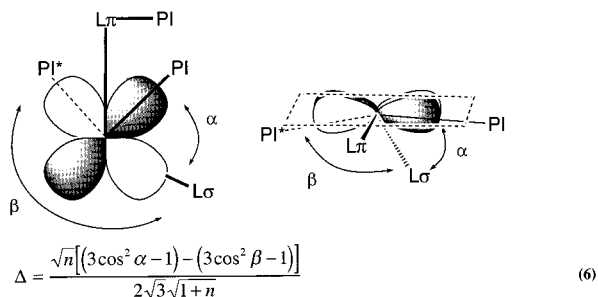
M−PI* is an image formed by rotating the M−PI vector by 90° in the PI−M−L$_\pi$ plane; α is the angle made by the M−PI and M−L$_\sigma$ vectors, and β is the angle made by the M−PI* and M−L$_\sigma$ vectors. n is the hybridization (of the type sd^n) of the metal orbital which makes a σ-bond with L$_\sigma$. β is determined trigonometrically from α, the PI−M−L$_\sigma$ angle ρ, and the L$_\sigma$−M−L$_\sigma$ angle ϕ. (This takes advantage of the inversion symmetry of the σ orbitals)

$$\beta = \arccos[(\sin\rho + \cot\rho\cos\rho)\cdot\cos\phi - \cot\rho\cos\alpha] \tag{7}$$

Thus, one pseudoatom defines both lobes of the π-bond, and all forces for both pseudo-$d\rho$ orbitals are passed though the ϕ, α, and ρ angles to the ligands and the single pseudoatom. The actual location of PI* is never calculated.

Once Δ is found, the pair defect energy is calculated as above, from eqs 2−4. The parameters (k) used to scale $\pi-\sigma$ bend energies were the same as that for the respective σ-bonds. This scaling assumes that overlap penalties for σ- and π-bonds at metal centers are similar in energy. The $\pi-\sigma$ bend energies are calculated for all angles involving σ- and π-bonds, including the σ- and π-bonds to the same center (L$_\pi$). This creates an energetic penalty if the angle made by Lπ−M and M−PI vectors is not 45° (in the above figure the angle is depicted at 45°). The use of default values for the overlap penalties of σ- and π-bonds at metal centers leads to a systematic overestimate of these energy terms which leads to consistently smaller L$_\pi$−M−L$_\sigma$ bond angles than those observed experimentally or by ab initio computations.

Modeling the $d\pi-d\pi$ overlap in a system with more than one π-bond proceeds in a similar, although more complex, fashion. The formula

depends on the four angles formed by the of the four component pseudo-$d\sigma$ orbitals as described below.
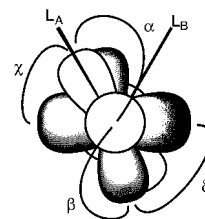
Let L$_A$ and L$_B$ represent ligands with M−L π-bonds; the M π-pseudoatoms are PI$_A$ and PI$_B$, respectively. Relevant bond angle defintions are: α is the π_A−M−π_B angle, ρA is the L$_A$−M−π_A angle, ρB is the L$_B$−M−π_B angle, ω is the L$_B$−M−L$_B$ angle, $\alpha L1$ is the L$_A$−M−π_B angle, and $\alpha 1L$ is the π_A−M−L$_B$ angle. The terms needed for overlap (Δ) computation are δ, χ, and β.

$$\delta = \arccos\left[\begin{array}{l}(\sin\rho A + \cot\rho A\cos\rho A) \\ \cdot[(\sin\rho B + \cot\rho B\cos\rho B)\cdot\cos\omega - \cot\rho B\cos\alpha L1] \\ - \cot\rho A\cos\beta\end{array}\right] \tag{8}$$

$$\chi = \arccos[(\sin\rho A + \cot\rho A\cos\rho A)\cdot\cos\alpha L1 - \cot\rho A\cos\alpha] \tag{9}$$

$$\beta = \arccos[(\sin\rho B + \cot\rho B\cos\rho B)\cdot\cos\alpha 1L - \cot\rho B\cos\alpha] \tag{10}$$

$$\Delta = \frac{[(3\cos^2\alpha - 1) - (3\cos^2\beta - 1)] - [(3\cos^2\chi - 1) - (3\cos^2\delta - 1)]}{6} \tag{11}$$

VALBOND Parameters. All parameters for the metals were taken from our previous hydride and alkyl study,[18] except: (1) the bending force constant for π bends, which was assumed to be equal to that for σ bends, and (2) a Bent's rule based "VALBOND parameter" which divides the s and d character among the σ-bonds. The VALBOND parameter was equal for carbon and hydrogen (1.0), and was assigned a value of 1.1 for nitrogen and oxygen, on the basis of NBO-calculated hybridizations of (NH)WH$_4$ and OWH$_4$ σ-bonds. Main group parameters were also taken from previous studies, except the main group to metal VALBOND parameters were set to 0.85, in recognition of the electropositive nature of metals and Bent's rule. One other parameter was modified, to add p character to lone pairs on N.

Structure Optimization. The starting structures used for VALBOND optimizations are either a DFT(B3LYP)-optimized structure or a crystallographic structure or a structure based on idealized bond angles associated with the σ-bond hybridization. For VALBOND computations on large molecules with available crystallographic structures, only the crystallographic structure was used as a starting point. Because the crystallographic structure is not necessarily the global minimum for the gas phase (especially with respect to torsional distortions), this procedure gives the most meaningful comparison between computed and observed structures. Pseudoatoms representing localized π orbitals were sketched in as necessary. All optimizations were carried out to a gradient rms <0.00001.

Supporting Information Available: A complete listing of the molecular mechanics potential energy functions; all DFT-computed geometries, vibrational frequencies, total energies, and NBO analyses; the optimized geometries of all VALBOND/UFF2 computations (PDF). This material is available free of charge via the Internet at http://pubs.acs.org.